difference between the site and the ecotone to the ordination value at the site; and (iii) a five-level moving average is plotted at the middle age. The measure of similarity is a correlation coefficient based on indicator pollen types. A description of this coefficient, and a list of the indicator pollen types, appears in O. K. Davis, *Rev. Palaeobot. Palynol.* **40**, 295 (1983).
18. J. R. Hastings and R. M. Turner, *The Changing Mile* (Univ. of Arizona Press, Tucson, 1965); W. H. Blackburn and P. T. Tueller, *Ecology* **51**, 841 (1970); J. W. Burkhardt and E. W. Tisdale, *ibid.* **57**, 472 (1976).
19. R. G. McMinn, *Ecology* **33**, 1 (1952); R. Daubenmire, *ibid.* **49**, 431 (1968).
20. The age of Rattlesnake Cave sediments is not known prior to 6760 years ago, because samples below a depth of 60 cm did not contain enough carbon to provide a reliable date (*15*). The age of the lower sediments is interpolated between 6760 years ago at 60 cm and 14,320 years ago at 175 cm. The later date is a minimum date based on the absence of Mount Mazama "S," which is present in sites of appropriate age in the area.
21. Subalpine meadow vegetation occurs where snowbanks last late (July) into the summer. In years when snow comes early or the snowbanks last until late, perennial vegetation surrounding the meadows is killed (*13*).
22. The shapes of the three curves are not crucial for the present discussion but may be of paleoclimatological interest. The low elevation ecotones were higher during the late glacial than today (Fig. 1). There are two possible explanations for this: (i) the late glacial steppe vegetation was qualitatively different from that of today or (ii) the late glacial climate may have been drier than today. On the basis of modern lapse rates in precipitation (*13*), the difference in elevation is equivalent to at least 10 to 20 mm less annual precipitation during the full glacial.
23. G. I. Smith and F. A. Street-Perrot, in *Late-Quaternary Environments of the United States*, H. E. Wright, Ed. (Univ. of Minnesota Press, Minneapolis, 1983).
24. R. S. Thompson, thesis, University of Arizona, Tucson (1984).
25. Smith and Street-Perrot (*23*) have shown that Searles Lake in southern California may have been deepest 11,000 years ago.
26. J. Iversen, *Dan. Geol. Unders. Afh. Roe KKe 2* **80**, 87 (1954).
27. G. R. Coope, *Philos. Trans. R. Soc. London Ser. B* **280**, 313 (1977).
28. J. F. Franklin, W. H. Moir, G. W. Douglas, C. Wiberg, *Arct. Alp. Res.* **3**, 215 (1971).

29 March 1984; accepted 15 May 1984

Uranus: Microwave Images

Abstract. *Observations of Uranus at wavelengths of 2 and 6 centimeters with the Very Large Array were made in 1980 and 1981. The resulting maps of brightness temperature show a subsolar symmetry at 2 centimeters but a near-polar symmetry at 6 centimeters. The 6-centimeter maps show an increase in temperature from equator to pole with some evidence for a warm "ring" surrounding the north pole. The disk-average temperatures (147 ± 5 K and 230 ± 6 K at 2 and 6 centimeters, respectively) are distinctly lower than recently reported values; these results suggest that the secular increase in temperature reported during the last 15 years has been reversed. The variations in brightness temperature probably reflect variations in ammonia abundance in the planet's atmosphere, but the mechanism driving these variations is still unclear.*

The microwave spectrum of Uranus is distinguished by two anomalies: a secular increase in brightness temperature during recent years and an apparent deficiency in ammonia opacity. Both of these features have been reviewed by Gulkis *et al.* (*1*), who have summarized observations from the last two decades, interpreted these results in terms of models for the atmosphere of Uranus, and predicted future trends in the planet's microwave brightness on the basis of these models. We present here the first fully resolved microwave images of Uranus, made with the Very Large Array (VLA) at wavelengths of 2 and 6 cm in 1980 and 1981. These images improve on the earlier VLA results of Briggs and Andrew (*2*), because more telescopes were available and we have observed at two frequencies. Our observations indicate that in contradiction to the prediction of Gulkis *et al.* (*1*)—that the brightness temperature of Uranus will continue to rise as the north pole becomes more visible—the maximum in the planet's microwave radiation has already occurred, before the pole reaches its closest sunward alignment in 1985. From our images we can directly assess the contribution of the pole to the measured average temperatures. We also find that there was a marked difference in the atmospheric opacity at 2 and 6 cm, as manifested by the differing symmetries of the brightness contours in the two images.

We observed Uranus at 6.1 and 2.0 cm during the May 1980 opposition and again at 6.1 cm during March 1981 (Table 1). We used the radio sources 1510-089 and 3C 286 to calibrate phase and flux, respectively. The assumed fluxes of 3C 286 were 7.41 Jy at 4.885 GHz and 3.44 Jy at 15.035 GHz (*3*).

After calibration, we constructed preliminary maps of the three fields, using standard National Radio Astronomy Observatory (NRAO) Fourier-transform programs. We then adjusted the phases of the 15-GHz data, which were in some cases affected by "seeing," to improve internal consistency, that is, we "self-calibrated" them, using an approximation of the preliminary map as a model of the true brightness distribution. A map of the second run was then made.

We "regularized" the three maps, using an algorithm implemented by F. Schwab of NRAO and W. Jaffe. This process reduces side lobes and other map artifacts and is thus similar to the more commonly used CLEAN and Maximum Entropy algorithms. It differs from these by implementing the specific constraint that the true sky emission is limited in extent. We assumed that no emission originates more than 1.5 planetary radii from the planet's center. This a priori assumption is consistent with the conclusion of Briggs and Andrew (*2*) regarding the absence of synchrotron emission at 6 cm beyond the limb of the planet. For display, the output maps were convolved with a Gaussian-function full width at half power of 0".75 in order to improve the temperature sensitivity of the results (at some loss of resolution) and to ensure a well-defined point spread function for later analysis.

The resulting maps are shown in Figs. 1 and 2. The 1981 map is not shown, since it essentially duplicates the 1980 map. Inspection of these figures reveals a distinctly different symmetry for brightness temperature (T_B) contours at the two wavelengths: at 2 cm the warmest spot on the planet is near the subsolar point, whereas at 6 cm the contours are symmetric about a point near the pole of the axis of rotation. This indicates that the temperature variations at 2 cm are caused by limb darkening only (*4*), whereas the 6-cm results reflect latitude changes in the radiation characteristics of the atmosphere. In Fig. 3 we plot the 6-cm T_B as a function of latitude, collected in bins of 15° of latitude near the pole and 30° near the equator.

A curious feature of Fig. 3 is the apparent T_B maximum some 30° off the north pole, representing a warm "ring" around the pole. Although the excess over the pole temperature is not extremely large, it also appears in the 1981 data. This feature may reflect a peculiar distribution of atmospheric opacity or it

Table 1. Observation log; IAT, International Atomic Time.

IAT date	IAT start time	Duration (hours)	Frequency (GHz)	Bandwidth (MHz)	Operating telescopes (No.)	Distance to Uranus (AU)
17 May 1980	$03^h\ 07^m$	10	15.035	50	20	17.74
18 May 1980	$03^h\ 03^m$	10	4.885	50	22	17.74
7 March 1981	$08^h\ 31^m$	10	4.885	50	26	18.50

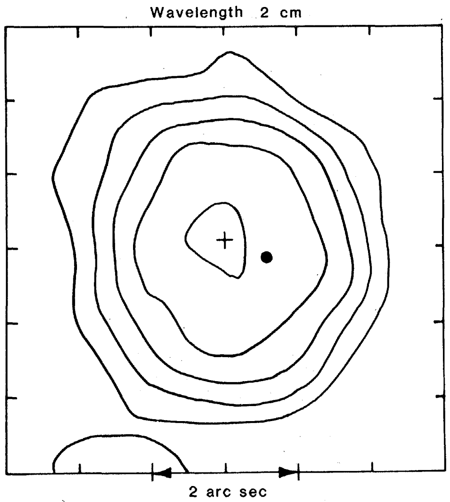

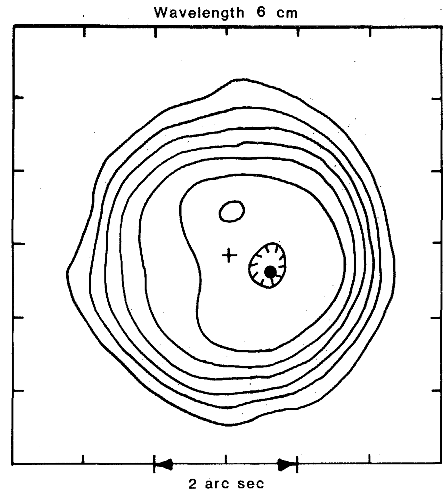

Fig. 1 (left). The May 1980 appearance of Uranus at 2 cm with a resolution of 0''.75. The optical diameter at this time was 3''.98. The contours of equal brightness temperature are in increments of 30 K and appear symmetric about the solar point, marked by the + sign. The dot marks the north rotation pole. The blob to the southwest is a noise fluctuation and does not represent real emission from the planet. Fig. 2 (right). The May 1980 appearance of Uranus at 6 cm with a resolution of 0''.75. The contours of equal brightness temperature are in increments of 40 K. The higher levels appear symmetric about the pole of rotation where there is a local temperature minimum, indicated by the hatched contour.

may be caused by synchrotron radiation from particles in a Uranian magnetic field (*5*).

In Table 2 we present the averaged planetary disk brightness temperatures (T_D) for the three observations. These are calculated from whole disk fluxes (*6*), based on a planetary equatorial radius of 25,650 km (*1*). The increase in measured temperature with increasing wavelength is entirely consistent with the extensive set of observations reviewed by Gulkis *et al.* (*1*). What is new here is the fact that both the 2-cm and the 6-cm temperatures are lower than recently measured values; the discrepancy is especially marked at 2 cm.

This finding contradicts the trend observed during the last 15 years, which suggested that T_D should continue to increase at least until 1985, when the pole faces the sun (*1*). Briggs and Andrew (*2*), using the VLA at 6 cm but with fewer telescopes, found $T_D = 259 \pm 4$ K in January 1978. Projecting to 1980 and using the values of Gulkis *et al.* (*1*) for the temperature drift, we would expect $T_D \sim 270$ K, some 40 K above our value. The 1973 and 1974 2-cm measurements by Gary (*7*) gave values of 185 K and 194 K, respectively, compared to our value of 147 K in 1980.

We agree with Briggs and Andrew (*2*) that the temporal variations in T_D cannot be explained in terms of changes in the geometrical aspect of Uranus alone. First, we find at 6 cm a pole-to-equator temperature drop of 80 ± 20 K (Fig. 3), in reasonable agreement with their value of 55 ± 20 K; in either case this is inadequate to explain the temporal variations. Second, we find no evidence of pole-to-equator variations at 2 cm, where the reported temporal change is larger than at 6 cm. Finally, we would expect geometry-induced effects to peak during 1985 when the pole is most nearly face on, while we in fact see a strong temperature decrease 5 years earlier.

At any observing frequency we probe the atmosphere down to a point where the ammonia density and the pressure-broadening of the line profile provide sufficient opacity at that frequency to generate the emission we observe. The 6-cm (4.9-GHz) measurements, which are farther from the ammonia line centers near 1.3 cm, probe to a greater depth and higher temperature (pressure ~15 bar) than the 2-cm (15-GHz) data (pressure ~5 bar). Our results indicate variations in the ammonia mixing ratio with time, latitude, and depth (*8*).

Table 2. Uranus microwave disk brightness temperatures.

Date	Wave-length (cm)	T_D (K)
May 1980	2.0	147 ± 5
May 1980	6.1	223 ± 6
March 1981	6.1	233 ± 6

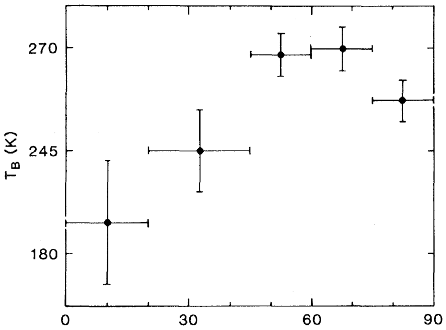

Fig. 3. Brightness temperatures at 6 cm as a function of planetary latitude for May 1980. The data have been averaged in bins indicated by the horizontal bars.

The higher temperatures near the pole in the 6-cm map (Fig. 3) probably indicate lower ammonia abundance there, allowing us to see into deeper, hotter layers. The decrease in T_D from 1978 to 1980 indicates a general increase in the ammonia abundance, although the increase seems more marked and more uniform at the higher (2-cm) level than at the 6-cm level.

Large changes in the ammonia distribution in a period much shorter than any in which the basic thermal structure of the atmosphere can change (*9*) require a "high gain" mechanism, one where a small relative energy change makes a large change in the ammonia vapor density. Two such mechanisms that have been suggested are changes in atmospheric circulation and an ammonia phase change (*1, 2*).

Both of these mechanisms have been discussed (*1, 2*), and they may be active simultaneously (*10*). We wish to point out, however, that no simple model can account for the observations, which have shown a steady increase in brightness temperature (decrease in ammonia abundance) over the last decade followed by a dramatic temperature decrease in 1980. This has occurred while the presumed driving force, solar heating on the polar regions, has changed slowly and monotonically. Possibly some of the early measurements of T_B are incorrect; the data compiled by Gulkis *et al.* (*1*) have been taken with different instruments, with different observing techniques, and over a long period, and they may contain systematic errors. If this is not the case, it is clear that we are far from understanding the dynamics of the Uranian atmosphere.

WALTER J. JAFFE
Space Telescope Science Institute, Homewood Campus, Baltimore, Maryland 21218
GLENN L. BERGE
Owens Valley Radio Observatory, California Institute of Technology, Pasadena 91125
TOBIAS OWEN, JOHN CALDWELL
Department of Earth and Space Sciences, State University of New York, Stony Brook 11794

References and Notes

1. S. Gulkis, E. T. Olsen, M. J. Klein, T. J. Thompson, *Science* **221**, 453 (1983).
2. F. H. Briggs and B. H. Andrew, *Icarus* **41**, 269 (1979).
3. One jansky (Jy) = 10^{-26}W m^{-2} Hz^{-1}.
4. W. Jaffe, G. Berge, J. Caldwell, T. Owen, *Bull. Am. Astron. Soc.* **13**, 732 (1981).
5. Neither Briggs and Andrew (*2*) nor we find evidence of such radiation away from the planet's limb. Synchrotron radiation is preferentially emitted perpendicular to magnetic field lines, however, and for a dipole field viewed nearly pole on the regions where the field is perpendicular to the line of sight may appear projected on top of the planetary disk. The steep spectrum normally associated with such emission would explain its absence at 2 cm.
6. We computed the disk fluxes by plotting the directly measured interferometer visibilities against projected base line. Extrapolating these plots to zero base line yields the estimated total flux. Noise contributes about ±2 K to estimated uncertainty, calibration uncertainties about ±3 K.
7. B. L. Gary, *Astron. J.* **79**, 318 (1974); personal communication to M. Klein, who normalized both years' observations to the current radius.
8. Another example of a change in opacity, this time at a much higher level in the atmosphere, is evident from photographs of the planet taken through a filter centered on the strong methane band at 890 Å. The appearance of Uranus has changed from that of an eccentric annulus with the darkest region near the subsolar point and the brightest region over the pole in 1976 to a uniformly illuminated disk in 1983 [B. A. Smith and H. J. Reitsema, in *Uranus and the Outer Planets*, G. E. Hunt, Ed. (Cambridge Univ. Press, New York, 1982), p. 173; B. A. Smith, personal communication].
9. P. H. Stone, *Space Sci. Rev.* **14**, 444 (1973); *Icarus* **24**, 292 (1975).
10. Only a few Amagat-centimeters of ammonia need change phase to produce the required opacity change. For typical ammonia-water ices, some 10^8 erg cm^{-2} are needed to vaporize this amount of material. This is less than 1 percent of the insolation at the pole in a 1-year period.

11. We thank K. Noll, I. de Pater, and S. Gulkis for helpful discussions and M. Klein for providing his unpublished compilation of microwave observation. This research was supported in part by NASA grants NGR33015141, 953614, NSG7320, and NGL 05-002-003 and NSF grant AST 79-11806A01. The Very Large Array is part of the National Radio Astronomy Observatory, which is operated by Associated Universities, Inc., under contract with the National Science Foundation.

23 February 1984; accepted 17 May 1984

The Fine Structure of Fossil Plant Cell Walls

Abstract. *The cell walls of sieve elements in the primary phloem of the Carboniferous fern* Tubicaulis *contain structural features that morphologically resemble cellulose microfibrils in extant plants. This may be the oldest example of distinct fibrillar structures in the fossil record. The possible identity and significance of these features are discussed and their structure is compared with that of cell walls in other fossil and extant plants.*

Phloem is the food-conducting tissue in vascular plants, and conducting cells (sieve elements) in this tissue have become adapted for transport by the loss or change of many cytoplasmic elements and the development of pores (sieve pores) in end and side walls. There are two basic types of sieve elements: sieve tube members, which occur almost exclusively in angiosperms, and sieve cells, which are found in gymnosperms and vascular cryptogams (ferns and related plants). The sieve cell is considered to be less specialized because it has diverged the least from a typical parenchyma cell (*1*). This is especially true of sieve cells in the vascular cryptogams, which are relatively small in diameter and only slightly elongate, with horizontal to somewhat oblique end walls (*2*). The perforated regions (sieve areas) are similarly developed on both side and end walls—a feature considered to represent the more primitive state (*1*).

The material we examined consists of petioles of the fern *Tubicaulis stewartii* (*3*) found in coal balls (calcium carbonate permineralizations) from Berryville, Illinois (*4*). Coal balls are known for their exceptional preservation of cellular detail in fossil plants (*5*) and have been found in Carboniferous coal seams in North America and Europe. Work on the phloem anatomy of *T. stewartii* petioles (*6*) has revealed features of the sieve cell walls that appear morphologically similar to cellulosic microfibrils in the cell walls of extant plants (*7*). This discovery provides the opportunity to examine some aspects of cell wall organization and structure in a plant approximately 290 million years old (Upper Pennsylvanian).

The phloem tissue in *T. stewartii* is unusual among the known fossil ferns (*6, 8, 9*), since it consists of several types of cells arranged in a very specific manner (Fig. 1A). The adaxial phloem (the tissue on the side of the petiole facing the main axis) consists of sieve cells approximately 10 μm in diameter and phloem parenchyma. The abaxial phloem (away from the axis) contains a single row of large sieve cells approximately 90 μm in diameter and at least 2.5 mm long (arrows in Fig. 1A). Since the cells taper gradually, it is difficult to distinguish end walls from side walls.

Where two of these large cells are adjacent, the common wall is covered with crowded, circular thin areas about 7.5 μm in diameter. Since this diameter is comparable to that of sieve areas in extant plants (*1*), these circular areas are interpreted as being sieve areas. However, the resolution obtained with light microscopy is inadequate to show sieve pores in these areas, which is necessary to confirm their identification as sieve areas.

Preparation of the fossils for scanning electron microscopy required the removal of the mineral matrix by selective etching (*9*). Since the cell walls are delicate, they often collapse after etching (Fig. 1B). The sieve areas on the larger cells are conspicuous, and appear as large circular to oval depressions (Fig. 1, B and C). Each of these areas is surrounded by a border of wall material (Fig. 1C), believed to have resulted from the collapse of cell walls during etching, and consists of numerous randomly arranged fibrils less than 0.1 μm in diameter (Fig. 1D). Spaces about 0.1 μm in diameter are visible between the individual fibrils (Fig. 1D). Microfibrils in extant plants are generally around 10.0 nm in diameter (*7*). However, it is impossible to measure the fibrils in the fossil material with this level of accuracy since they cannot be sectioned for transmission electron microscopy. The size of the fibrils as determined with the scanning electron microscope is at best a rough estimate because of distortion due to tilting of the specimen and the added thickness of the gold coating. Although the chemical nature of these fibrils is unknown, it is unlikely that they represent calcium carbonate artifacts, since this substance would have been removed during etching.

The appearance of the wall areas is nearly identical to that of primary pit fields on the walls of parenchyma cells and developing sieve elements in extant plants (*7*). In sieve cells the primary pit fields develop into sieve areas by enlargement of the plasmodesmata-sized perforations to form sieve pores. These pores are often ringed with depositions of callose that appear early in development and generally remain at maturity (*1, 10*). In vascular cryptogams the sieve pores are often so small at maturity as to be almost indistinguishable from plasmodesmata (*2*). In addition, some vascular cryptogams do not deposit callose at any time during their development (*11*). Thus it is sometimes difficult to distinguish sieve elements and parenchyma cells, even in living plants. The problem is compounded in fossils by poor preservation, crushing of cells, and the inability to view the material in a functioning state.

The size and shape of the large cells in *Tubicaulis* phloem indicate that they represent sieve cells and not parenchyma cells, although the sieve areas more closely resemble primary pit fields than mature sieve areas. The fibrillar areas may represent primary pit fields in im-